JOURNAL OF SPACECRAFT AND ROCKETS
Vol. 45, No. 2, March–April 2008

Multibody Orbit Architectures for Lunar South Pole Coverage

Daniel J. Grebow,* Martin T. Ozimek,* and Kathleen C. Howell†
Purdue University, West Lafayette, Indiana 47907-2045
and
David C. Folta‡
NASA Goddard Space Flight Center, Greenbelt, Maryland 20771

DOI: 10.2514/1.28738

A potential ground station at the lunar south pole has prompted studies of orbit architectures that ensure adequate coverage. The creation of multibody orbit constellations begins with an investigation of periodic orbits in the circular restricted three-body problem. A detailed analysis of halo and vertical families, as well as other orbits near the libration points in the vicinity of the moon, suggests that constant communications can be achieved with two spacecraft in combinations of Earth–moon libration-point orbits. In particular, the investigation focuses on nine different orbits from these families with periods ranging from 7 to 16 days. Natural solutions are generated in a full-ephemeris model including solar perturbations. Possible ground stations on the moon and the Earth are established for coverage results and verification of communications capabilities. Preliminary station-keeping costs are also computed for long-term communications with the ground stations.

Nomenclature

D	=	displacement along the unstable direction
M	=	state-relationship matrix
$\boldsymbol{R}$, $\boldsymbol{V}$	=	three-element position and velocity vectors along the reference spacecraft path, km, km/s
$\tilde{\boldsymbol{R}}$, $\tilde{\boldsymbol{V}}$	=	three-element position and velocity vectors along the actual spacecraft path, km, km/s
T	=	time to complete one period of orbital motion, s
TOF	=	time of flight, s
t	=	nondimensional time
$\boldsymbol{X}^{W_u}$	=	vector defining the unstable direction associated with the state-transition matrix over a full period
x, y, z	=	barycentric coordinate axes in the rotating frame of the primaries (nondimensional)
x^m, y^m, z^m	=	moon-centered coordinate axes in the rotating frame of the primaries (nondimensional)
$\hat{Y}^{W_u}$	=	unstable eigenvector associated with the state-transition matrix over a full period
$\lambda_{\max}$	=	maximum eigenvalue from the state-transition matrix over a full period
μ	=	nondimensional mass parameter
ν	=	stability index of a periodic orbit
$\boldsymbol{\Phi}$	=	state-transition matrix

I. Introduction

ONE current focus of autonomous and manned exploration studies is the region near the south pole of the moon due to the potential existence of frozen volatiles [1,2]. Since the President's Vision for Space Exploration announcement in January 2004, NASA has indicated that water ice at the lunar poles may help facilitate exploration of the solar system [3]. NASA's exploration, communication, and navigation systems team (specifically, the Lunar Communications and Navigation Systems Group) is interested in spacecraft architectures for communications with ground stations on the lunar surface. Such a ground station on the moon requires a system of satellites that is always in view of the Earth and that can provide constant communications between the lunar surface and the Earth. Various ideas are now being considered to support this concept. On a broad scale, for example, NASA's Living with a Star program was created to learn more about the sun–Earth system [4]. The initiative included the possible investigation of north and south "pole-sitters" for constant Earth atmospheric monitoring and surveillance. Such ideas may be adaptable to the moon for feasible south pole architectures. Studies of satellite constellations in Earth orbit are also being examined for application to the moon.

The potential use of libration-point orbits for lunar south pole coverage has not yet been fully investigated. However, an infinite variety of periodic solutions exist in the restricted three-body problem. Many of these families of orbits have been studied extensively by engineers, mathematicians, and astrophysicists (including Szebehely [5], Zagouras and Kazantzis [6], Breakwell and Brown [7], Robin and Markellos [8], Howell and Breakwell [9], and Dichmann et al. [10]). Because of the nature of the solutions, some useful architectures for lunar coverage may exist within the context of the three-body problem. Using a multibody model to design trajectories for communications between the far side of the moon and the Earth was discussed by Farquhar [11,12] as early as 1967, for example. Libration-point orbits are investigated here to create architectures for continuous coverage of the south pole of the moon with only two spacecraft [13]. The initial design phase originates in the circular restricted three-body problem (CR3BP). Vertical orbits, introduced by Moulton [14] in 1920, and other L_1 and L_2 families of orbits are investigated. The families are computed via a variable-time targeting scheme [7]. Orbits are selected from these families based on 1) time to complete one full period and 2) feasibility for lunar south pole coverage. Once the specific architecture is selected, the orbit is discretized into a series of patch points. With modifications to a corrections scheme posed by Wilson and Howell [15], the patch points are then differentially corrected to meet both the desired time of flight and orbit periodicity requirements. The solutions are transitioned to the full-ephemeris model, including solar perturbations, using the Purdue University software package Generator [16].

Presented at the AAS/AIAA Space Flight Mechanics Meeting, Tampa, Florida, 22–26 January 2006; received 6 November 2006; revision received 13 April 2007; accepted for publication 16 April 2007.

*Graduate Student, School of Aeronautics and Astronautics, Armstrong Hall, 701 West Stadium Avenue. Student Member AIAA.

†Hsu Lo Professor of Aeronautical and Astronautical Engineering, School of Aeronautics and Astronautics, Armstrong Hall, 701 West Stadium Avenue. Associate Fellow AIAA.

‡Senior Flight Dynamics Engineer, Building 11, Room S116. Senior Member AIAA.

Since the announcement of the near-term space exploration agenda, interest in the lunar south pole region has served as a focus for constellation design studies. Ely and Lieb [17,18] have investigated the placement of a system of satellites to support a south pole station and global orbital constellations using a two-body model with the gravitational perturbations of a third body. An approximate disturbing function for the third body (i.e., the Earth) is averaged, and frozen orbit conditions are computed with Lagrange's planetary equations. The conditions are then integrated in the full model, including solar radiation pressure. Alternatively, initially modeling the orbits in the CR3BP includes any higher-order perturbing effects of the Earth (otherwise neglected), and a differential corrections scheme ensures that the orbits remain close to the prescribed path in the full-ephemeris model.

The long-term station-keeping costs are also an important factor in determining the feasibility of these systems. In 1971, Farquhar's [12] investigation of the use of halo orbits to maintain a continuous communications link between a lunar ground facility and the Earth also included an examination of the station-keeping costs. Later, extensive work on optimal station-keeping strategies using Floquet modes for halo orbits in the Earth–moon system was completed by Simó et al. [19,20]. In this approach, the unstable subspace that is available from dynamic systems theory is used to develop a station-keeping strategy. Station-keeping analyses for Earth–moon halo orbits were also completed by Howell and Pernicka [21], Howell and Keeter [22], and Gómez et al.[23]. Most recently, Scheeres et al. [24] and Renault and Scheeres [25] have investigated the generalized optimal placement of statistical control maneuvers applied to orbits in the Earth–moon restricted three-body problem. The orbits in these studies are typical of those that might be used for lunar coverage and also provide an additional benchmark for the station-keeping costs. Adapting models created by Folta and Vaughn [26], the patch points that define a libration-point orbit from Generator are targeted in Satellite Tool Kit® (STK). Then a facility is placed at the Shackleton crater (89.9 deg S, 0.0 deg E) near the south pole of the moon, and access times between the facility and the dual-spacecraft chain are analyzed. Access times between the spacecraft and potential Earth-based transmitting sites are also computed for a possible communications relay to the Shackleton site. Finally, a preliminary station-keeping analysis in STK is accomplished.

In summary, this work was originally motivated by the requirements for trajectory options in the design of a lunar constellation composed of a minimum number of spacecraft, to simultaneously maintain communications between a facility at the lunar south pole and the Earth. To support such a mission, a variety of orbits must be available for flexibility; the design process must be fast, efficient, and automated. The resulting strategy is based on a multibody model and generates trajectories that maintain various communications and coverage requirements. The solutions are ultimately transitioned to a full-ephemeris model with solar perturbations. For a given scenario, access times and station-keeping costs are evaluated for comparisons.

II. Periodic Orbits and the Circular Restricted Three-Body Problem

The circular restricted three-body model describes the motions of three bodies subject to their mutual gravitational forces. The primary gravitational bodies move about their barycenter on circular paths. The third body (i.e., the spacecraft) is assumed to possess negligible mass in comparison to the primaries. The rotating x axis is defined along the vector between the primaries; the z axis is parallel to the angular velocity vector associated with the Keplerian primary orbits. Then the usual barycentric system of equations describing the motion of the third body are written

$$\ddot{x} = 2\dot{y} + x - \frac{(1-\mu)(x+\mu)}{d^3} - \frac{\mu[x-(1-\mu)]}{r^3}$$
$$\ddot{y} = -2\dot{x} + y - \frac{(1-\mu)y}{d^3} - \frac{\mu y}{r^3}, \qquad \ddot{z} = \frac{-(1-\mu)z}{d^3} - \frac{\mu z}{r^3} \tag{1}$$

where x, y, and z are the components of the third-body position relative to the rotating barycentric frame. The mass parameter is μ; then d and r are the relative distances between the third body and the first and second primaries, respectively. The equations are nondimensional, and the characteristic quantities are the total mass, the distance between the primaries, and the magnitude of the system angular velocity.

The state-transition matrix $\boldsymbol{\Phi}(t_f, t_0)$, associated with Eq. (1), is also available. By analyzing endpoint variations, $\boldsymbol{\Phi}(t_f, t_0)$ can be employed in an iterative process to yield the exact initial conditions for periodic motion in the CR3BP. From a first-order Taylor series expansion, the general form of a time-varying targeting scheme for convergence becomes

$$\begin{Bmatrix} \delta \boldsymbol{R}_f \\ \delta \boldsymbol{V}_f \end{Bmatrix} = \begin{bmatrix} \boldsymbol{\Phi}(t_f, t_0) & \dot{\boldsymbol{R}}_f \\ & \dot{\boldsymbol{V}}_f \end{bmatrix} \begin{Bmatrix} \delta \boldsymbol{R}_0 \\ \delta \boldsymbol{V}_0 \\ \delta(t_f - t_0) \end{Bmatrix} \tag{2}$$

where $\boldsymbol{R} = \{x \;\; y \;\; z\}^T$ and $\boldsymbol{V} = \{\dot{x} \;\; \dot{y} \;\; \dot{z}\}^T$. The columns of $\boldsymbol{\Phi}(t_f, t_0)$ are associated with the desired control parameters [i.e., $\delta \boldsymbol{R}_0$ and $\delta \boldsymbol{V}_0$, $\delta(t_f - t_0)$], and the rows correspond to the endpoint constraint parameters [7,13]. The control parameters are iteratively updated by variations in the initial state until the endpoint constraints are fully satisfied. Furthermore, once a single periodic solution is determined, neighboring solutions in the same family are computed using a method of continuation over an additional constraint parameter. The method is extrapolated to determine complete families of periodic orbits.

A. Halo Orbits, Vertical Orbits, and Other L_1 and L_2 Families of Periodic Orbits

Using the targeting scheme, families of L_1 and L_2 periodic halo and vertical orbits are quickly generated. In addition, a family of orbits that bifurcates from a near-rectilinear halo orbit is also obtained. Specific members of the orbit families are isolated based on both the communications instrument and subsurface constraints, bounding the useful range of orbits within a family to those with lunar altitudes between 50 and 100,000 km. (That is, solutions not within these altitude constraints are disregarded.) Furthermore, it is useful to redefine the orbits in a moon-centered rotating frame such that

$$x^m = x - (1-\mu), \qquad y^m = y, \qquad z^m = z \tag{3}$$

A number of L_1 and L_2 southern halo orbits appear in Fig. 1. These two families are particularly effective in this problem because the motion is almost always within line of sight to the Earth. Most recently, the halo-orbit families have been thoroughly investigated by Farquhar [12], Breakwell and Brown [7], Howell and Breakwell [9], Gómez et al. [27], and Dichmann et al. [10]. The halo orbits investigated here resemble both the traditional halo shape and the highly elliptic, near-rectilinear motion, with a passage very close to the moon. For almost the entire period of the motion, a spacecraft in any near-rectilinear halo orbit possesses a line of sight to the lunar south pole.

Vertical orbits are doubly symmetric orbits near the libration points and, in the y–z projection, resemble a figure eight in shape, as seen in Fig. 2. Since Moulton [14] highlighted their existence in 1920, the nonlinear vertical orbits have been extensively investigated by Zagouras and Kazantzis [6] and most recently by Dichmann et al. [10]. The complete families are attainable using a method of continuation with a targeting scheme based on Eq. (2). As the family continues, larger-amplitude vertical orbits encompass both primaries. However, only vertical orbits with altitudes less than 100,000 km are incorporated as options for coverage of the lunar poles. These orbits bend toward both the north and south poles of the moon, a favorable characteristic for polar coverage.

An additional family also includes orbits that remain in view of the lunar south pole for significant intervals of time. Some of these orbits possess characteristics similar to the near-rectilinear halo orbits. The orbits bifurcate from a six-day near-rectilinear L_2 halo orbit and might be described in terms of a butterfly shape (see Fig. 3).

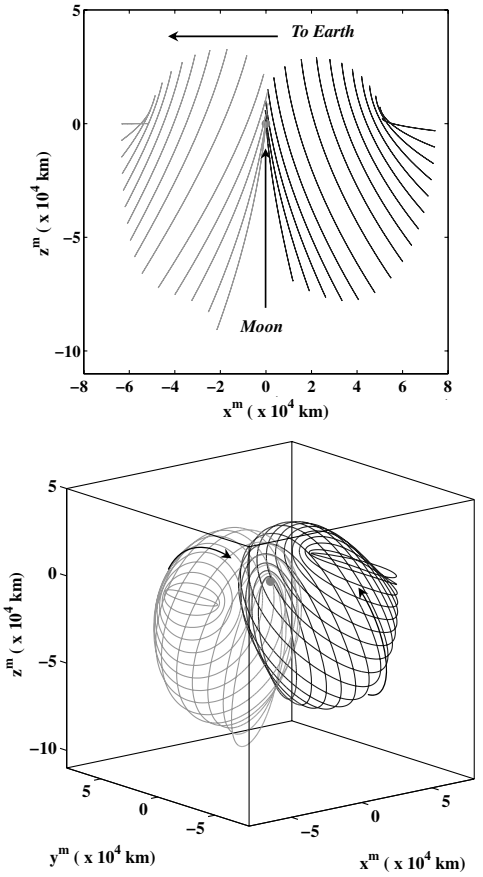

Fig. 1 Southern halo-orbit families: Earth–moon L_1 (left) and L_2 (right).

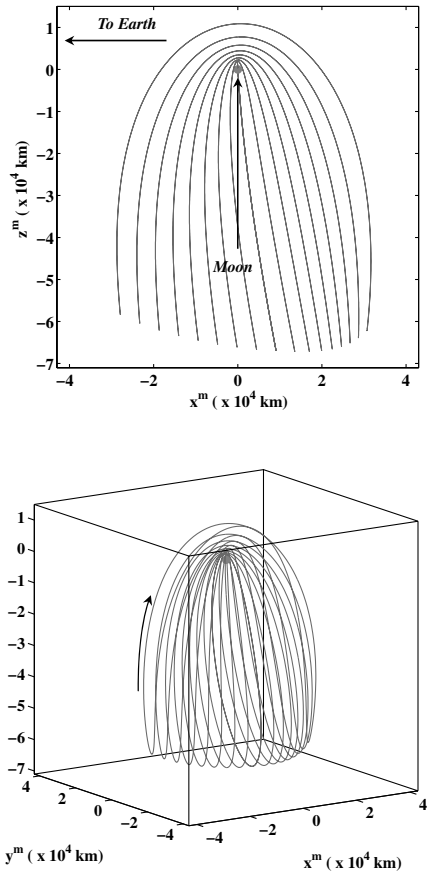

Fig. 3 Southern L_2 butterfly-orbit family.

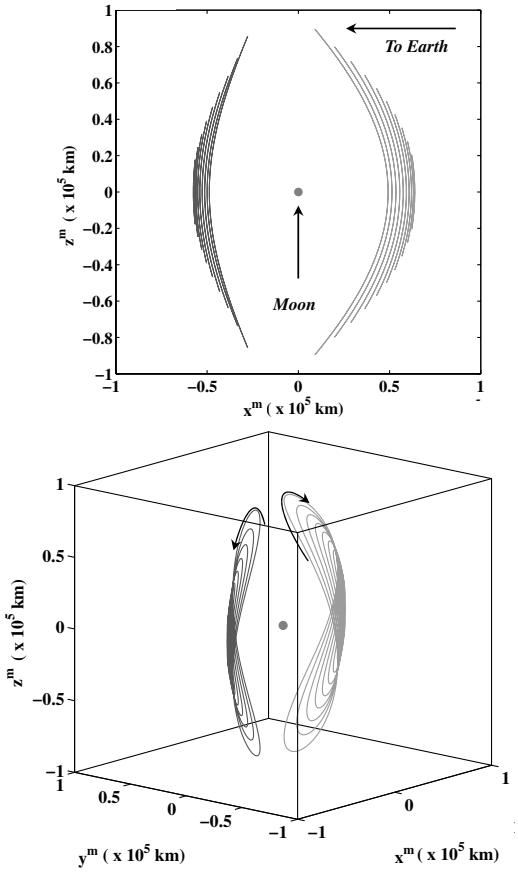

Fig. 2 Vertical-orbit families of interest: Earth–moon L_1 (left) and L_2 (right).

Comparable motions around the smaller primary have been documented by Robin and Markellos [8]. Similar to vertical orbits, the motion in a butterfly orbit resembles a figure eight; however, these orbits wrap around both the near and far sides of the moon, such that a direct line of sight to the lunar south pole exists for nearly the entire orbital period.

B. Orbit Selection Criteria

The time to complete one full period is a useful selection parameter in the initial design phase. Let the maximum excursion distance, as defined by Eq. (3), be the maximum x^m distance for each orbit in the moon-centered rotating frame. Orbital periods are plotted against maximum excursion distance during initial design selection, as indicated in Fig. 4 (top). Suitable regions for the production of feasible architectures occur when the orbital periods are commensurate. One such region consists of orbits in L_1 and L_2 halo families sharing periods between 7.9 and 12.2 days. An example that exhibits feasible south pole coverage consists of a 12-day L_1 and 12-day L_2 halo-orbit combination, illustrated by the heavy dashed line in Fig. 4 (top). Another region with commensurate combinations consists of orbits with a ratio of periods equal to 2:1; that is, one period is exactly twice that of the other. Note that L_2 halo orbits with periods between 6.0 to 7.2 days exhibit this behavior with the entire L_2 butterfly-orbit family. This is not actually surprising when the shapes of the orbits are viewed in Figs. 1–3. An example from this region consists of a 14-day L_2 butterfly-orbit and a seven-day L_2 halo-orbit combination, as noted by the two light dashed lines in Fig. 4 (top). This information also serves as a basis for the determination of many other commensurate orbit combinations that lead to complete south pole coverage. Furthermore, orbits not investigated here may be added to Fig. 4 without affecting the analysis.

Also useful for design purposes is the stability index ν. The stability index, corresponding to one orbit period T, is defined as

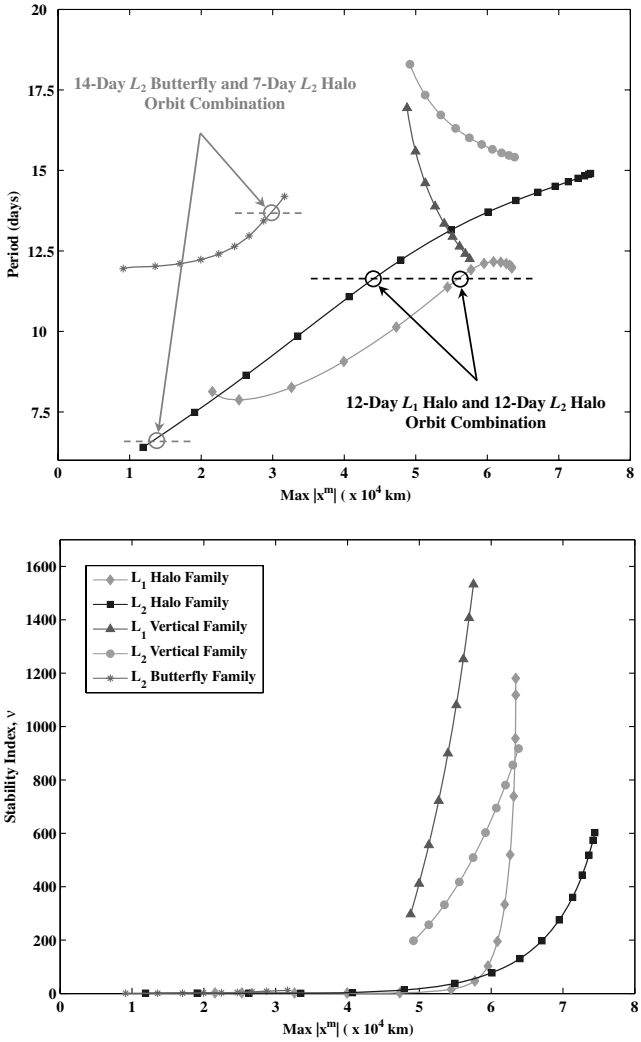

Fig. 4 Period (top) and stability index (bottom) versus maximum x^m distance from the moon.

$$\nu = \frac{1}{2}\left(|\lambda_{\max}| + \frac{1}{|\lambda_{\max}|}\right) \tag{4}$$

where $\lambda_{\max}$ is the maximum eigenvalue from the monodromy matrix $\boldsymbol{\Phi}(T+t,t)$, computed at the end of one revolution. A stability index of one indicates a stable orbit, whereas stability indices greater than one reflect instability. Of course, a large stability index indicates a divergent mode that departs from the vicinity of the orbit very quickly. Generally, the stability index is directly correlated to the station-keeping costs and inversely related to transfer costs. The stability indices for orbits from the various families appear in Fig. 4 (bottom) as functions of maximum excursion distance from the moon. In general, the stability index increases with distance from the moon.

Using periodicity and stability criteria, orbits from Figs. 1–3 are selected for use in a coverage scenario. Either a single orbit is selected and two spacecraft are placed in the same orbit (but out of phase) or a unique orbit is selected for each spacecraft such that their periods are commensurate. When an orbit with a precisely defined period is desired, a modified two-level differential corrections scheme accepts the patch points of a previously generated neighboring orbit as an initial guess and iterates to generate an orbit with the specified period. When this process is complete for all desired orbits, patch points for multiple revolutions are added to develop a baseline 180-day mission. Once the final trajectories are obtained, the initial time corresponding to one of the two spacecraft is phase-shifted by a half-period, thus allowing the greatest chance for complete coverage of the lunar south pole.

C. Modified Two-Level Differential Corrector

In 1988, Howell and Pernicka [28] used a two-level differential corrections scheme to determine continuous quasi-periodic motion near the libration points in the CR3BP. The two-level process has more recently been modified to include multiple flight regimes by Wilson and Howell [15] and Hughes et al. [29]. The first level of the corrections scheme employs Eq. (2) to target positions defined in terms of discretized state vectors, or patch points, along the desired orbit. The second phase, or level, computes small variations in the patch-point positions and times to minimize the velocity discontinuities at each of the first-level patch points. Iterations continue until the intermediate velocity variations $\delta \boldsymbol{V}$ are reduced to zero and a natural solution is identified. The current work, as detailed by Grebow [13], uses the targeter created by Howell and Pernicka [28], adapted to incorporate constraints as posed by Wilson and Howell [15].

Using Wilson and Howell's [15] notation, there exists a state-relationship matrix $\mathbf{M}$, such that the smallest Euclidean norm yields the new variations in position $\delta \boldsymbol{R}_i$ and time δt_i, corresponding to the ith patch point: that is,

$$\begin{Bmatrix} \delta \boldsymbol{R}_1 \\ \delta t_1 \\ \vdots \\ \delta \boldsymbol{R}_n \\ \delta t_n \end{Bmatrix} = [\mathbf{M}]([\mathbf{M}][\mathbf{M}]^T)^{-1} \begin{Bmatrix} \delta \boldsymbol{V}_2 \\ \vdots \\ \delta \boldsymbol{V}_{n-1} \end{Bmatrix} \tag{5}$$

where $\delta \boldsymbol{V}_i$ represents the internal discontinuity in the velocity vector (to be minimized) from the first level of the corrections procedure for n patch points. The components of the state-relationship matrix $\mathbf{M}$ are derived from the linear variational equations relating consecutive patch-point states.

The method can also be adapted to compute $\delta \boldsymbol{R}_i$ and δt_i subject to additional constraints. Development of the periodicity constraint, for example, appears in Marchand et al. [30] and Grebow [13]. A sample implementation is incorporated in Marchand and Howell [31]. For this analysis, the orbit must be periodic, and a specified time-of-flight (TOF) condition must be satisfied as well. Therefore, Eq. (5) becomes

$$\begin{Bmatrix} \delta \boldsymbol{R}_1 \\ \delta t_1 \\ \vdots \\ \delta \boldsymbol{R}_n \\ \delta t_n \end{Bmatrix} = [\mathbf{M}^*]([\mathbf{M}^*][\mathbf{M}^*]^T)^{-1} \begin{Bmatrix} \delta \boldsymbol{V}_2 \\ \vdots \\ \delta \boldsymbol{V}_{n-1} \\ \boldsymbol{R}_n - \boldsymbol{R}_1 \\ \boldsymbol{V}_n - \boldsymbol{R}_1 \\ \text{TOF} - (t_n - t_1) \end{Bmatrix} \tag{6}$$

where the matrix $\mathbf{M}^*$ in Eq. (6) includes the partial derivatives of *all* imposed constraints with respect to position and time. That is, $\mathbf{M}^*$ is simply the augmented state-relationship matrix $\mathbf{M}$ in Eq. (5), including the partial derivatives of $\boldsymbol{R}_n - \boldsymbol{R}_1$, $\boldsymbol{V}_n - \boldsymbol{R}_1$, and TOF $-$ $(t_n - t_1)$ with respect to $\delta \boldsymbol{R}_i$ and δt_i (see Marchand et al. [30] for a general formulation of the matrix $\mathbf{M}^*$). Thus, $\delta \boldsymbol{V}_i$, $\boldsymbol{R}_n - \boldsymbol{R}_1$, $\boldsymbol{V}_n - \boldsymbol{R}_1$, and TOF $-$ $(t_n - t_1)$ are *all* simultaneously minimized iteratively until the periodic orbit that satisfies the required time-of-flight condition is obtained.

D. Invariant Manifold Theory and the Unstable Subspace

Information concerning the unstable subspace is available from analysis of the phase space near a periodic orbit and is useful in a preliminary station-keeping analysis. For n patch points along a periodic orbit, in which the first and last patch points coincide, the monodromy matrix for the ith point along the orbit is computed as

$$\begin{aligned} &\boldsymbol{\Phi}(T + t_i, t_i) \\ &= [\boldsymbol{\Phi}(t_{i+n}, t_{i+n-1})][\boldsymbol{\Phi}(t_{i+n-1}, t_{i+n-2})] \cdots [\boldsymbol{\Phi}(t_{i+2}, t_{i+1})][\boldsymbol{\Phi}(t_{i+1}, t_i)] \end{aligned} \tag{7}$$

where $T = t_{i+n} - t_i$ is the time to complete one full period. Let the

six-dimensional vector $\hat{Y}_i^{W_u}$ represent the eigenvector associated with the unstable mode from $\Phi(T + t_i, t_i)$, such that it can be written in terms of three-dimensional components $\boldsymbol{R}_i^{W_u}$ and $\boldsymbol{V}_i^{W_u}$ as

$$\hat{Y}_i^{W_u} = \begin{Bmatrix} \boldsymbol{R}_i^{W_u} \\ \boldsymbol{V}_i^{W_u} \end{Bmatrix} \tag{8}$$

Then the unstable direction is represented by

$$\boldsymbol{X}_i^{W_u} = \frac{\hat{Y}_i^{W_u}}{R_i^{W_u}} \tag{9}$$

A small perturbation in the unstable direction $\boldsymbol{X}_i^{W_u}$ places the spacecraft on an unstable manifold departing the vicinity of the reference solution. The perturbing terms are represented by

$$\begin{Bmatrix} \delta\boldsymbol{R}_i \\ \delta\boldsymbol{V}_i \end{Bmatrix} = D \cdot \boldsymbol{X}_i^{W_u} \tag{10}$$

where D is an initial displacement in the unstable direction. The unstable manifold is obtained by perturbing each patch-point state by $\pm\{\delta\boldsymbol{R}_i^T \;\; \delta\boldsymbol{V}_i^T\}^T$ and integrating forward in time. This information is useful for station-keeping analysis in general. In this study, it was incorporated into a STK analysis.

III. Advanced Modeling in Generator and Satellite Tool Kit

All orbits are initially designed under the assumption that a spacecraft is subject only to the gravitational forces of the Earth and moon in the CR3BP. High-fidelity software that more accurately represents the force models and perturbing motions is desired to ensure complete coverage of the lunar south pole and provide preliminary station-keeping costs. For this reason, the Purdue University software Generator and AGI's STK are used to precisely model and analyze all coverage schemes of interest.

A. Full-Ephemeris Modeling with Purdue University Software Package Generator [16]

The Purdue University software package Generator is a mission design tool that is based on multibody equations of motion, including solar perturbations. Preliminary baseline trajectories can quickly be determined within the context of the two-, three-, or four-body problem. Any number of bodies and ephemeris information can be incorporated as desired (other forces, control schemes, and design components are available but not employed here). For this application, the 180-day baseline orbits acquired by using the modified two-level differential corrector in the CR3BP are transferred to the Generator full-ephemeris model. The patch-point velocity discontinuities are minimized within Generator and a modified orbit emerges. The resulting coverage schemes are initially analyzed by examination of the z^m displacement of each spacecraft at the same instant of time. The z^m displacement reflects the out-of-plane component of the position vector. The potential to maintain line of sight to the lunar south pole exists only if at least one of the spacecraft is below the Earth–moon fundamental plane $z^m = 0$ at all times. Consider two spacecraft in a single L_1 halo orbit. A typical two-spacecraft coverage scheme is achieved by displacing the motion of each spacecraft by a half-period. Thus, the two spacecraft are then phase-shifted in the L_1 halo orbit, and the z^m displacement of each spacecraft as a function of time appears in Fig. 5. The dashed line highlights the z^m value at which the two spacecraft possess a common z^m component but are moving in opposite directions along the orbit. The dashed line in Fig. 5 demonstrates that the z^m crossing occurs significantly below the fundamental plane, ensuring that at least one spacecraft is always within direct line of sight to the south pole. The first goal is to maximize the distance between the dashed line and the fundamental plane ($z^m = 0$). This initial step does not fully account for the actual position of the lunar south pole due to the tilt and nutation of the rotation axes, but it provides an estimate for the line-of-sight coverage behavior over time. Additionally, analyzing the z^m displacement in this way also offers a visual confirmation that the proper periodicity constraint is implemented correctly.

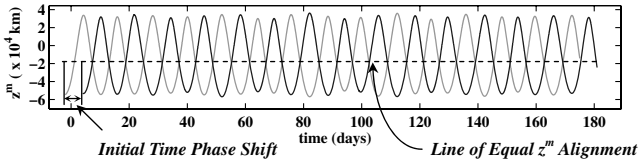

Fig. 5 Displacement of z^m in the rotating reference frame for two spacecraft in 12-day L_1 halo orbits.

B. Station-Keeping and Coverage Analyses in Satellite Tool Kit

Station-Keeping. Once a baseline coverage scenario is constructed, potential station-keeping costs are investigated. Adapting a model created by Folta and Vaughn [26], patch points along the orbits from Generator are targeted in STK using the Astrogator® model and Astrogator Connect. The propagator in the targeting sequence is an eighth-order, full Runge–Kutta–Verner integrator with ninth-order error control, including solar perturbations. Targeting Generator patch points in this slightly different model implies that small corrections are required at each point. In general, however, transitioning from Generator to Astrogator results in corrections of less than 1 m/s per year. (Of course, these corrections could be removed with slight adjustment to the orbits. However, because the magnitude of the corrections is significantly smaller than the costs associated with station-keeping due to "real" errors, this step is not deemed necessary.)

A preliminary station-keeping analysis is constructed by modifying the targeting sequence in Astrogator Connect. The station-keeping algorithm for four patch points appears in Fig. 6.

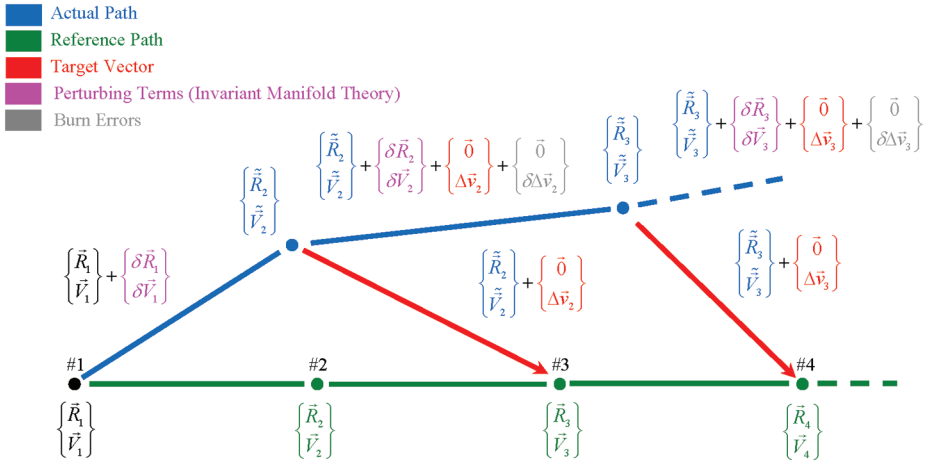

Fig. 6 Schematic for station-keeping algorithm.

Note that the green path represents the reference orbit as computed directly from Generator. Along the green path, the patch points from Generator are indicated as dots and are defined as the target points in Astrogator (i.e., $\{\boldsymbol{R}_i^T \;\; \boldsymbol{V}_i^T\}^T$). The vehicle is not actually associated with the reference state, of course. Perturbing the spacecraft into the unstable subspace and determining the maneuvers necessary to offset the error and maintain the orbit ultimately yields a good approximation of the maximum station-keeping cost [19–24]. So the perturbations along the unstable direction are computed from Eq. (10) and appear in magenta as $\{\delta\boldsymbol{R}_1^T \;\; \delta\boldsymbol{V}_1^T\}^T$. Recall that position and velocity perturbations are represented by the displacement D along the unstable direction in Eq. (10). These perturbations might represent navigation errors, for example, and the impact of such errors is most significant if they are in the unstable direction. The magnitude of D is sized to be consistent with the magnitude of some average navigation 3σ position errors; thus, the value might typically cover a range from 2 to 3 km in position. To account for slight differences between the unstable directions in the CR3BP and the full model, a baseline 3σ position error of 5 km is used in this analysis. These perturbations $\{\delta\boldsymbol{R}_1^T \;\; \delta\boldsymbol{V}_1^T\}^T$ are added to the initial state, and propagation in Astrogator over the time interval necessary to reach point 2 moves the vehicle along a new actual path (in blue). Of course, the state associated with the spacecraft at the end of this propagation is actually $\{\tilde{\boldsymbol{R}}_2^T \;\; \tilde{\boldsymbol{V}}_2^T\}^T$. A correction maneuver $\Delta\boldsymbol{v}_2$ is computed via a targeting sequence in Astrogator to actually reach target point 3. (This $\Delta\boldsymbol{v}_2$ is representative of the cost to offset the error introduced via $\{\delta\boldsymbol{R}_1^T \;\; \delta\boldsymbol{V}_1^T\}^T$.) The $\Delta\boldsymbol{v}_2$ from the targeting sequence is adjusted by $\pm 2\%$ to include hot $(+)$ or cold $(-)$ burn errors $\delta\Delta\boldsymbol{v}_2$. However, to incorporate possible errors, perturbations along the unstable direction are again added. After the adjusted $\Delta\boldsymbol{v}_2 + \delta\Delta\boldsymbol{v}_2$ is implemented, the spacecraft is perturbed $\{\delta\boldsymbol{R}_2^T \;\; \delta\boldsymbol{V}_2^T\}^T$ in the unstable direction and again propagated forward. The process then continues for a specified time interval (i.e., a predetermined number of target points). The total station-keeping cost is the sum of the $\|\Delta\boldsymbol{v}_i\|$.

Coverage. A full lunar south pole coverage analysis is also available using STK. Because of constant exposure to sunlight and possibly the existence of frozen volatiles, the lunar south pole is a likely location for a ground station on the moon. In addition, current interest is directed at exploration options expanding out from the south pole. One such location that is of scientific interest is the Shackleton crater. Therefore, a facility is placed on the moon with coordinates of 89.9 deg S and 0.0 deg E, corresponding to the Shackleton site. Assuming an omnidirectional communications link, the spacecraft is only accessible to the facility if it is within a direct line of sight. Intervals when the facility is unable to access either spacecraft are recorded. Both spacecraft are placed in a constellation and the times when either or both spacecraft have line-of-sight access with the facility are computed via an access chain. Furthermore, information from the facility regarding each spacecraft during the access times is available. For example, a plot of the elevation angle of each spacecraft from the facility as a function of time appears in Fig. 7. The plot demonstrates that the desired coverage is achieved. From Fig. 7, it is apparent that at least one spacecraft is always 15 deg above the horizon as viewed from the facility. That is, constant communication is achieved anywhere *inside* the Shackleton crater, assuming the walls of the crater are inclined to no greater than 15 deg.

IV. Architectures for Lunar South Pole Coverage

For this investigation, nine different orbits from the families represented in Figs. 1–3 are selected based on their periods (see Fig. 4). Coverage can be adequately ensured with two spacecraft in just one of these nine orbits by phasing the vehicles appropriately. However, as already noted, selecting orbits with commensurate periods allows for architectures with combinations of two *different* orbits for complete lunar south pole coverage. For example, rather than placing two spacecraft in the same seven-day L_2 near-rectilinear halo orbit, use one spacecraft in a seven-day L_2 near-rectilinear halo and the other vehicle in a 14-day L_2 butterfly orbit. The combination may provide more complete coverage. Possible orbits for use in combination to ensure lunar south pole coverage are represented in Table 1. Recall that a lunar facility is placed at the site of the Shackleton crater. In addition, three fictional ground stations are placed in a new configuration along the Earth equator separated by 120 deg. The line-of-sight access between the ground-based Earth stations and the spacecraft constellation is computed via another access chain. The results are representative of access between the Earth and the spacecraft (i.e., times when the Earth can communicate with either spacecraft). It might be more accurate for actual mission analysis to specify a real transmitting site on the Earth for ground station communications with the lunar-based spacecraft. A potential location for this ground station is the White Sands Test Facility (WSTF), located in New Mexico (32.3 deg N, 106.8 deg W). Although a 180-day baseline mission is selected for this study, the general process can be extended for longer time spans without, in general, affecting the results. Of course, longer mission times will require greater computational effort. However, because the orbit is discretized into a series of patch points, the computational time can be drastically reduced by integrating the segments in parallel.

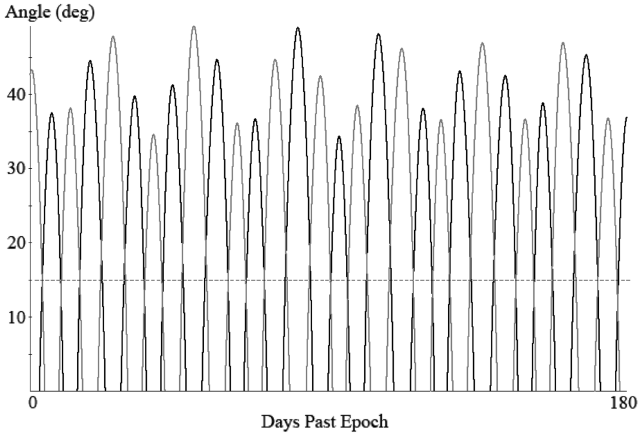

Fig. 7 Elevation of each spacecraft above the horizon as viewed from the Shackleton crater facility vs days past epoch for the 12-day L_1 halo-orbit scenario.

A. Sample Case: Two 12-Day L_1 Halo Orbits

One possible solution to the coverage problem employs two spacecraft in the same 12-day L_1 halo orbit. The lunar periapsis altitude for this orbit is approximately 36,500 km. One spacecraft is phase-shifted by a half-period, thus allowing the greatest chance for lunar south pole coverage, and the relative spacecraft positions appear in Fig. 8. Fifteen revolutions are added for the baseline 180-day mission.

The orbits are transitioned to the full model. Because of the prescribed phasing, at least one spacecraft is always 19,500 km below the Earth–moon fundamental plane, ensuring coverage of the lunar south pole (recall Fig. 5). The orbits for the two spacecraft that result from Generator appear in Fig. 9 in both a moon-centered rotating system of coordinates and the inertial mean J2000 frame. Note that the trajectory of one spacecraft is plotted as a bold line and the motion of the other spacecraft appears lighter. The quasi-periodic

Table 1 Potential orbits for coverage of the lunar south pole

Orbit type	Libration point	Period, days	Stability index
Near-rectilinear halo	L_2	7.0	1.00
Near-rectilinear halo	L_1	8.0	1.25
Near-rectilinear halo	L_2	8.0	1.00
Halo	L_1	12.0	60
Halo	L_2	14.0	115
Vertical	L_1	14.0	690
Butterfly	L_2	14.0	11.3
Vertical	L_1	16.0	370
Vertical	L_2	16.0	515

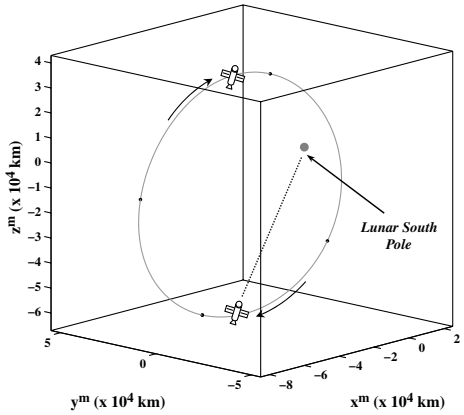

Fig. 8 Twelve-day L_1 orbit and patch points (black dots) from CR3BP.

motion of the spacecraft is most apparent in the Earth–moon rotating frame, in which both orbit trajectories follow nearly the same path. Note that the patch-point positions (dots) were adjusted for continuous motion in the full-ephemeris model. In the inertial mean J2000 frame, the motion of the spacecraft appears to "umbrella" around the moon.

Targeting these Generator patch points in Astrogator (without any additional errors) using Astrogator Connect requires less than 0.41 m/s over 15 revolutions in total corrections for each spacecraft. The station-keeping analysis is performed by perturbing the spacecraft in STK using a 3σ value of 5 km along the unstable direction that is determined from the CR3BP phase-space analysis. The corresponding mean 3σ velocity perturbation is 3.82 cm/s (recall $\{\delta \boldsymbol{R}_1^T \quad \delta \boldsymbol{V}_1^T\}^T$ in Fig. 6). To remain close to the nominal path, a maneuver is implemented every second patch point. Thus, for the baseline 180-day mission, each spacecraft implements a maneuver every six days of average size 1.11 m/s. The total maximum $\Delta \boldsymbol{v}$ for each spacecraft is 31.17 m/s, including the 2% burn errors.

Table 2 Percent access times for 12-day L_1 halo orbits

Configuration	Facility at Shackleton crater	Earth	Facility at WSTF
Only satellite 1	63.51%	100.00%	48.26%
Only satellite 2	63.92%	100.00%	48.17%
Both satellites	27.42%	100.00%	44.61%
Either satellite	100.00%	100.00%	51.82%

As demonstrated in Fig. 7, there is a spacecraft between the elevation angles of 0 and 15 deg, 27.42% of the simulation time (see Table 2). When the elevation angle of one spacecraft relative to the facility decreases to around 15 deg, the elevation angle of the line-of-sight vector to the other spacecraft appears above the horizon, for complete access anywhere inside the crater (providing the walls are inclined less than 15 deg). In this way, one spacecraft trades access times with the facility while the other spacecraft passes over the northern hemisphere of the moon. Incorporated in Fig. 7 and Table 2 is the direct access with the true exact location of the ground facility (89.9 deg S, 0.0 deg E), including lunar libration from wobble and nutation of the spin axis. Even with the inclusion of lunar nutation and inclination with respect to the Earth–moon fundamental plane, at least one spacecraft is always directly within line of sight of the south pole.

Each spacecraft always maintains line of sight with at least one ground station 100% of the simulation time. Of course, this is also evident from Fig. 10, in which each spacecraft is visibly always in direct line of sight with the Earth. Such a result is expected for

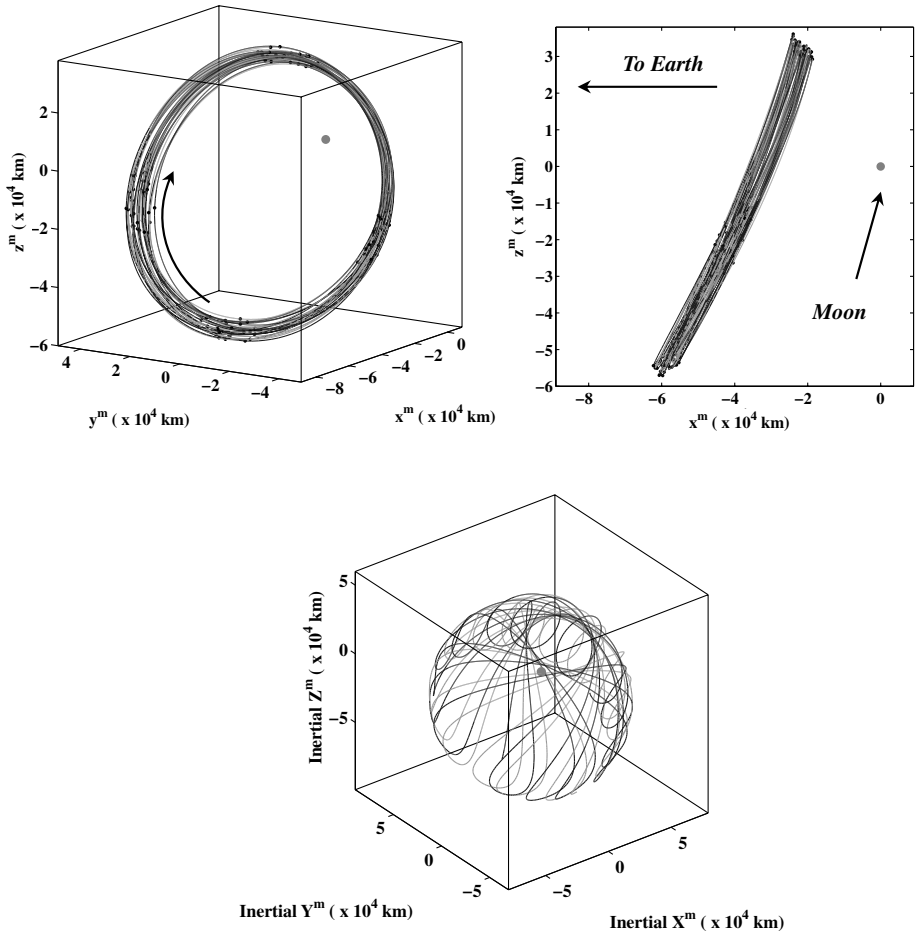

Fig. 9 Two phased spacecraft in 12-day L_1 halo orbits from Generator: moon-centered rotating reference frame (top left), x^m–z^m projection (top right); inertial mean J2000 reference frame (bottom).

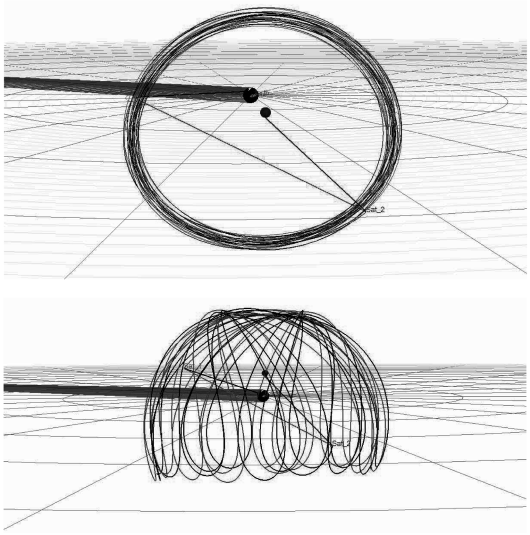

Fig. 10 STK 12-day L_1 halo orbits with access beams: moon-centered rotating frame (top); moon-centered inertial mean J2000 frame (bottom).

spacecraft in Earth–moon halo orbits [11]. A chain is created for access between the spacecraft constellation and a facility located at WSTF (Fig. 10, beams departing the figure frame). The times when each spacecraft, either spacecraft, or both spacecraft possess line of sight with the facility are computed. Also, as evidenced from Table 2, each spacecraft maintains line of sight for nearly half the simulation time. Given Earth rotation, this is reasonable. As depicted with the beam between the spacecraft in Fig. 10, a final communications link between the spacecraft also provides valuable information. A spacecraft in direct line of sight with the lunar facility may not, at the same time, possess line of sight with WSTF. However, if the other spacecraft possesses line of sight in direct communications with WSTF, then a communications link is established between the lunar facility and WSTF via a relay between the two spacecraft (see Fig. 10). For some orbits, line of sight may not exist when the moon is between the spacecraft (i.e., when one spacecraft is at periapsis and the other is at apoapsis).

B. Other Combinations for Lunar South Pole Coverage

Besides two spacecraft in the same 12-day L_1 halo orbit, other combinations of various orbits from Table 1 also yield viable coverage options (see Figs. 11–15). Observe that Table 1 includes stability indices that are computed for each orbit. In general, smaller periapsis altitudes directly correlate to smaller stability indices. Also, smaller distances between the dashed line for equal z^m alignment and the fundamental plane, as computed in Generator, translate to smaller ranges over which the elevation angles of the two spacecraft allow simultaneous coverage scenarios in STK. A smaller range over the elevation angles reflects smaller time intervals over which the Shackleton crater facility has access with both spacecraft. Furthermore, nearly all the coverage scenarios possess nearly 50% access with WSTF (see Tables 3–7).

The L_2 seven-day halo-orbit combination, with the orbits plotted in Figs. 11a and 11b, uses only one halo orbit for both spacecraft. This near-rectilinear orbit passes approximately 2750 km from the lunar surface at periapsis, 72,100 km at apoapsis altitude, and possesses a stability index of 1.00. Analyzing the Generator z^m displacement components, the scenario results in a distance between the dashed line for equal z^m alignment and the fundamental plane of 55,000 km (see Fig. 11a). Both spacecraft simultaneously achieve access with the lunar facility for elevation angles from 0 to 65 deg for 92.78% of the simulation time. Therefore, if the walls of the Shackleton crater are less than a 65-deg incline, constant communications can be maintained anywhere inside the crater. In Fig. 11b, an instant when both spacecraft are accessed by the Shackleton facility is apparent; that is, both moon-to-spacecraft access beams are active. Because the seven-day L_2 halo orbit is near-rectilinear, the motion is similar to a highly elliptical two-body orbit. Therefore, during the majority of the orbital period, both spacecraft are within direct line of sight of the lunar facility, leading to large periods of redundant coverage. In fact, one spacecraft possesses line of sight with the Shackleton facility over 95% of the simulation time (see Table 3). Furthermore, the spacecraft are fully accessible from the Earth 100% of the time, with only small intervals when one spacecraft cannot communicate with the other due to interference with the moon. That is, for 99.21% of the simulation time, the spacecraft possess direct line of sight with each other.

The eight-day L_1 and L_2 halo-orbit scenario depicts an orbit combination that uses halo orbits about two distinct libration points (Fig. 12). Like the seven-day scenario, the eight-day L_1 and L_2 halo orbits offer low minimum altitudes at approximately 1400 and 6000 km, with apoapsis altitudes of 90,200 and 76,900 km, and stability indices of 1.25 and 1.00, respectively. The Generator analysis of Fig. 12a (bottom) demonstrates that the minimum distance between the dashed line for equal z^m alignment below the fundamental plane is 60,000 km. Because of these similarities, simultaneous coverage of the lunar facility is achieved at approximately 0 to 60 deg in elevation angle, as apparent in Fig. 12c. That is, at least one spacecraft is always 60 deg above the horizon. Table 4 shows that the spacecraft configured in the eight-day L_1 halo orbit is in direct line of sight with the Shackleton facility nearly 99% of the simulation time. As with the previous scenarios using halo orbits, spacecraft placed in the eight-day L_1 and L_2 halo orbits are always in direct access with the Earth. The spacecraft possess line of sight with one another 99.73% of the simulation time.

The 16-day L_1 and L_2 vertical-orbit scenarios also use multiple libration-point orbits (Fig. 13). The periapsis altitudes are much larger than the near-rectilinear halo orbits at 48,600 and 55,800 km, respectively. The corresponding apoapsis altitudes are approximately 82,100 km for the L_1 vertical orbit and 69,600 km for the L_2 vertical orbit. Because of the nature of the figure-eight shape, no two-spacecraft combination exhibits complete coverage of a south pole facility, as is apparent in Fig. 13b. Neither spacecraft is within direct line of sight of the Shackleton facility when both spacecraft cross the fundamental plane at the same time. The elevation plot in Fig. 13c confirms that there are small intervals (i.e., 1.39% of the simulation time) when the lunar facility cannot access either spacecraft. At this same instant, the moon passes directly between the spacecraft, and therefore the spacecraft are also not able to communicate with each other. In fact, the STK results plotted in Fig. 13b reveal an instant in time when no access beams exist between the lunar facility and either spacecraft. At this same instant, an access beam also does not exist between the two spacecraft. Spacecraft-to-spacecraft line of sight occurs only 94.33% of the simulation time. Furthermore, due to passage behind the moon, L_2 vertical orbits do not possesses 100% line-of-sight access with the Earth. However, because the out-of-plane motion for the vertical orbit is larger than the halo orbits, the verticals are able to communicate with WSTF nearly 52% of the time (see Table 5).

The orbits for two spacecraft in a single 14-day L_2 butterfly orbit appear in Figs. 14a and 14b. As with the near-rectilinear halo-orbit scenarios, motion along a butterfly orbit remains primarily within direct line of sight of the facility throughout the orbit, with a low periapsis altitude of approximately 8800 km. The corresponding apoapsis altitude for this orbit is approximately 67,900 km. However, these orbits possess a greater stability index than that of the near-rectilinear halo orbits. As seen in Fig. 14a, the Generator minimum z^m displacement crossing occurs 36,000 km below the fundamental plane. Figure 14c demonstrates that at least one spacecraft is always 45 deg above the horizon. That is, there is simultaneous coverage between 0 and 45 deg and, from Table 6, this occurs 78.25% of the time. For 0.39% of the simulation time, the moon interferes with communication between the spacecraft. Similar to a spacecraft in an L_2 vertical orbit, a spacecraft in a 14-day L_2 butterfly orbit passes behind the moon and therefore does not possesses 100% line of sight with the Earth (although a slightly different phasing is possible).

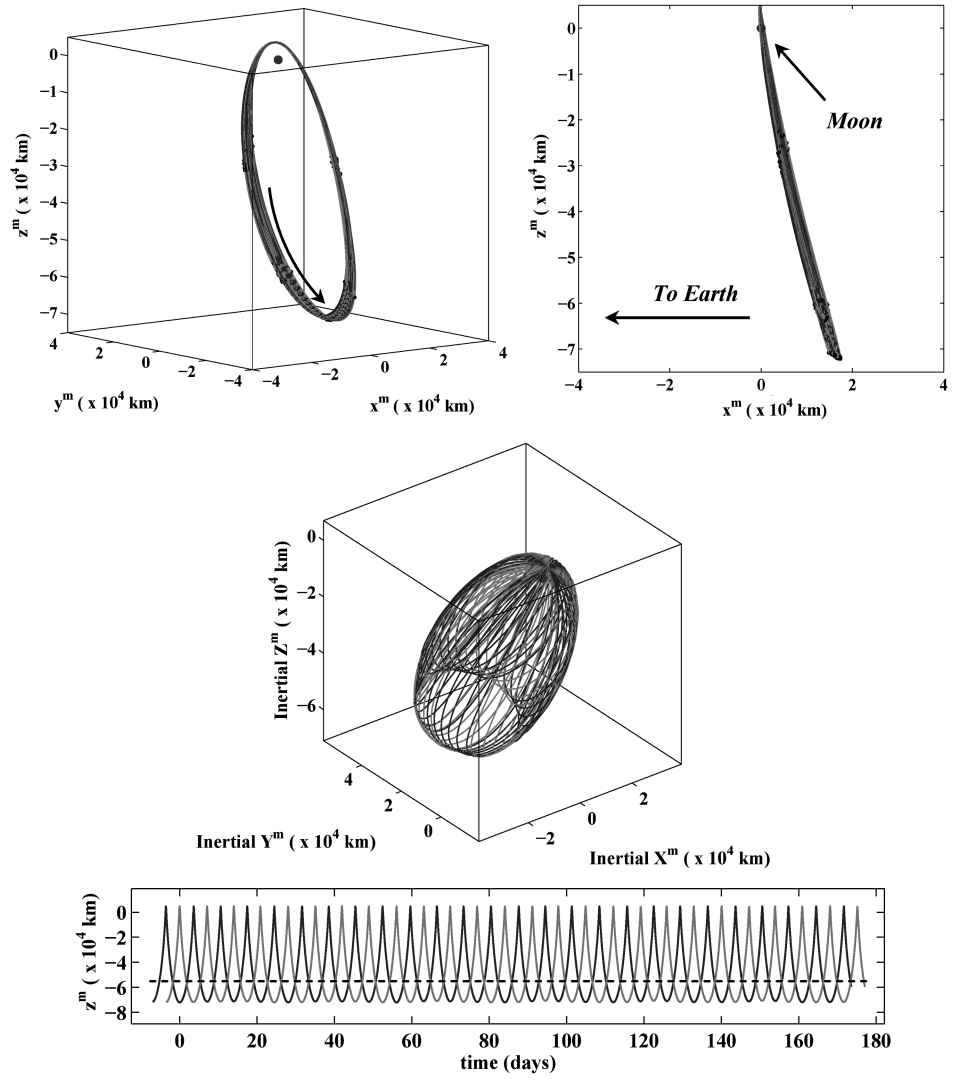

a)

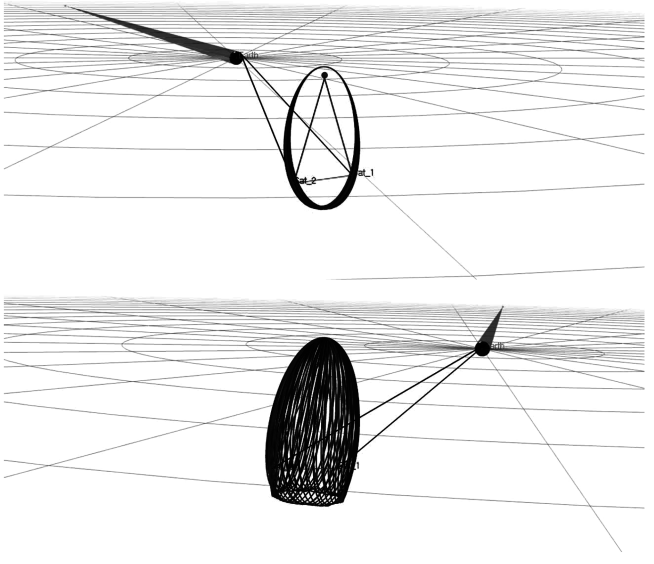

b)

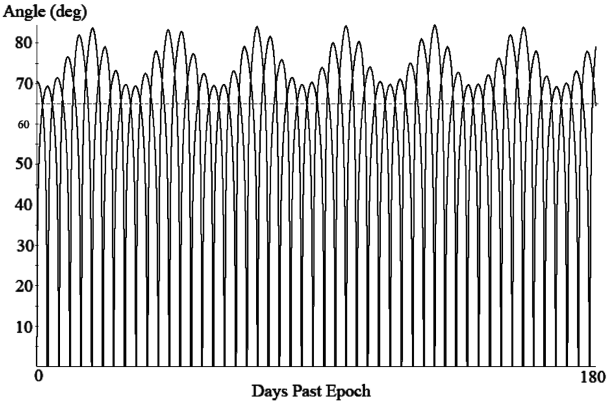

c)

Fig. 11 Seven-day L_2 halo orbits: a) two phased spacecraft in orbits from Generator: moon-centered rotating reference frame (top left), x^m-z^m projection (top right), inertial mean J2000 reference frame (center), and z^m displacement from rotating reference frame (bottom); b) STK results: moon-centered rotating frame (top) and moon-centered inertial frame (bottom); and c) elevation of each spacecraft above the horizon as viewed from the Shackleton crater facility vs days past epoch.

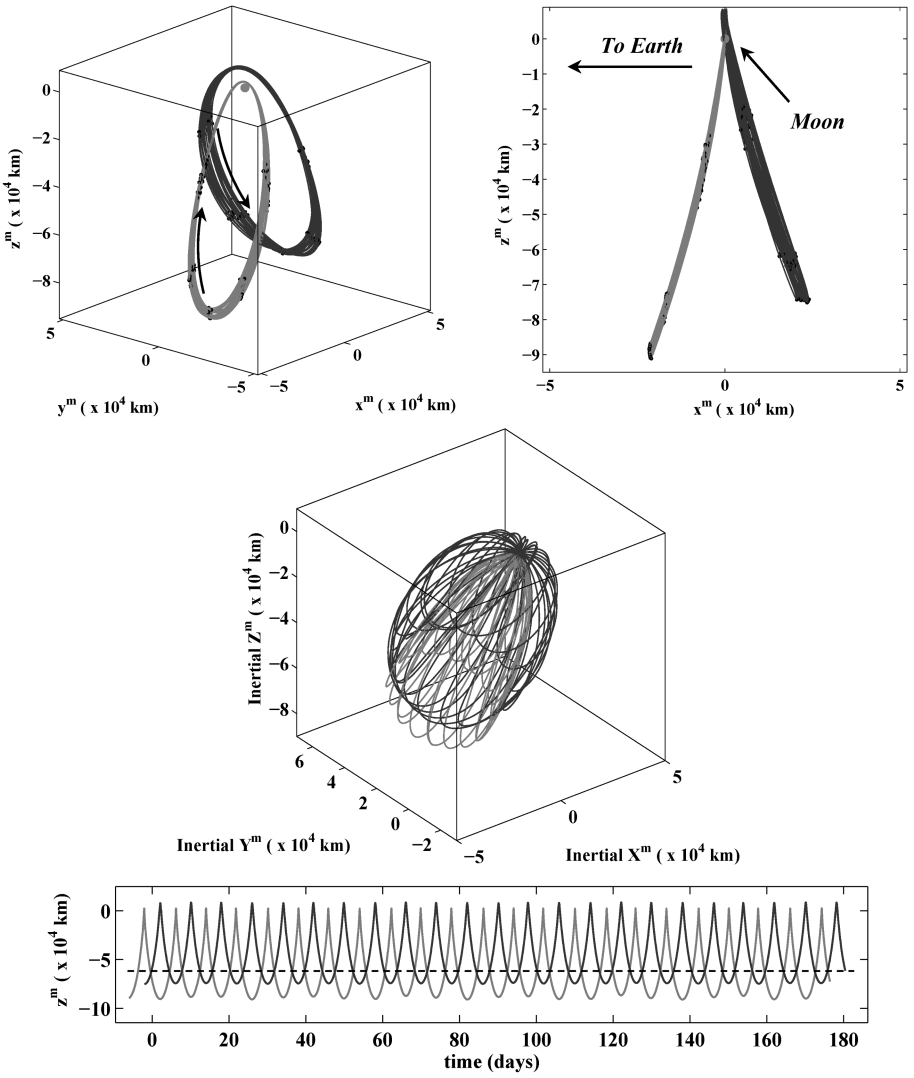

a)

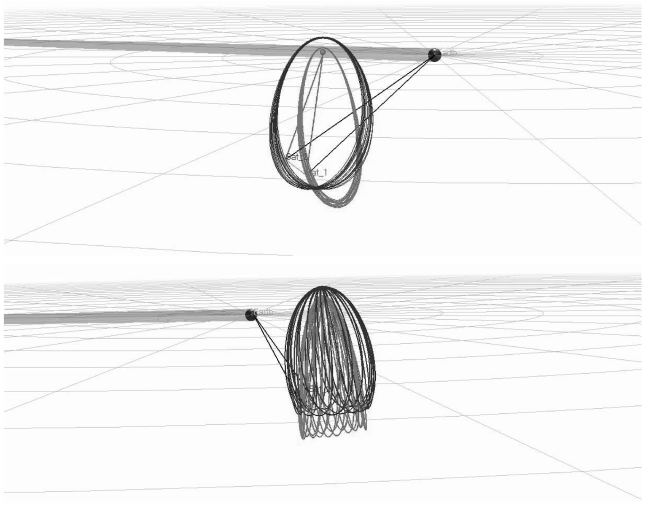

b)

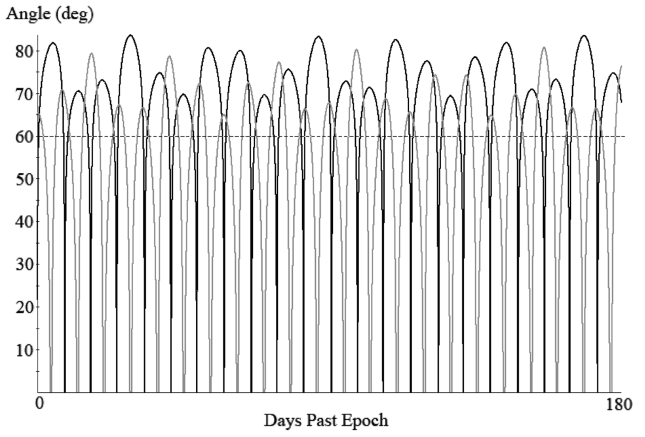

c)

Fig. 12 Eight-day L_1 and L_2 halo orbits: a) two phased spacecraft in orbits from Generator: moon-centered rotating reference frame (top left), x^m-z^m projection (top right), inertial mean J2000 reference frame (center), and z^m displacement from rotating reference frame (bottom); b) STK results: moon-centered rotating frame (top) and moon-centered inertial frame (bottom); and c) elevation of each spacecraft above the horizon as viewed from the Shackleton crater facility vs days past epoch.

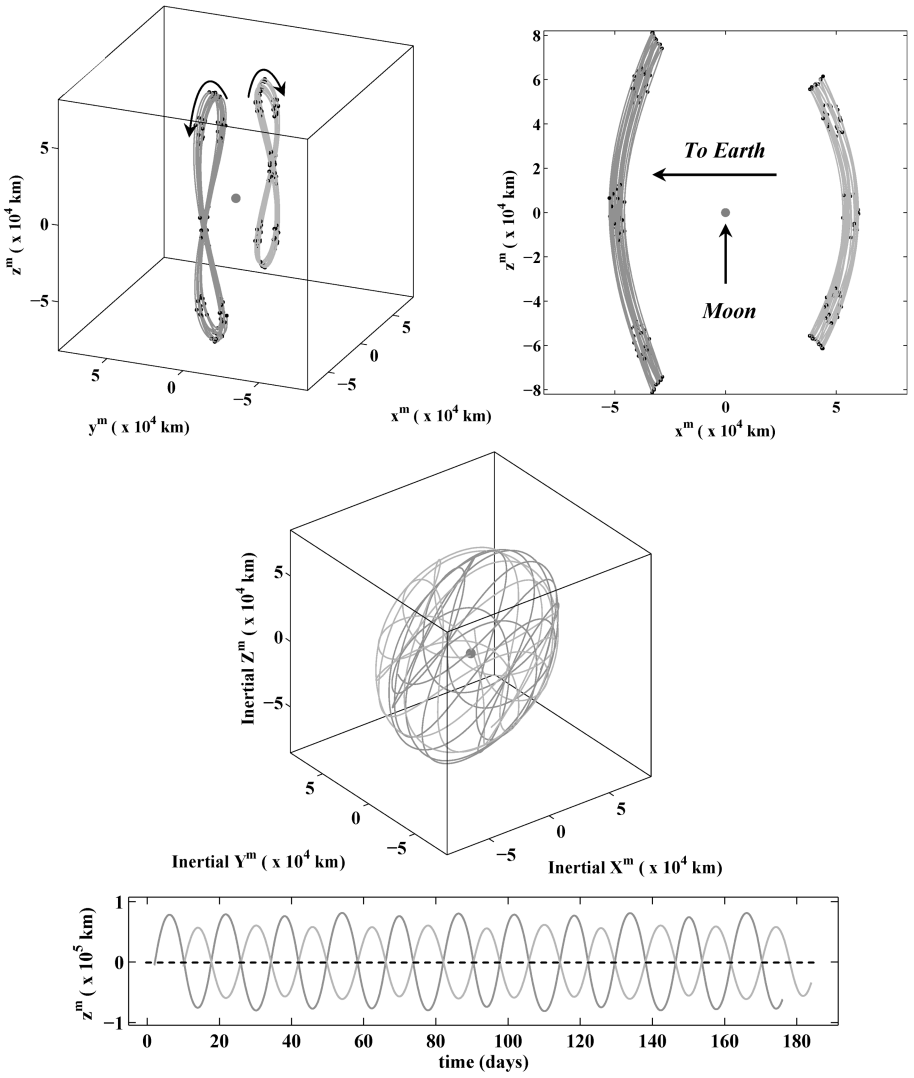

a)

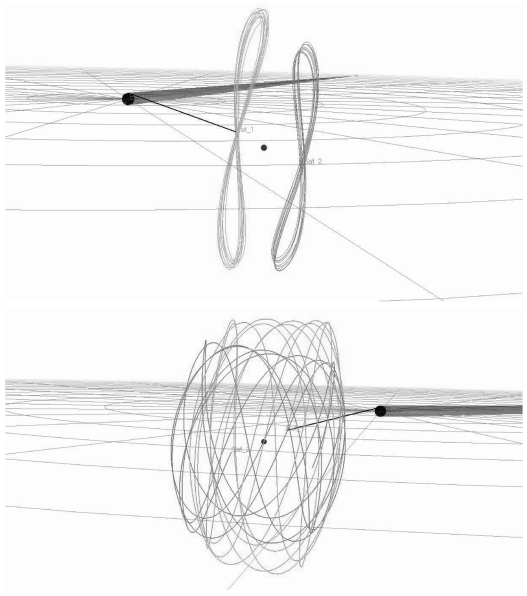

b)

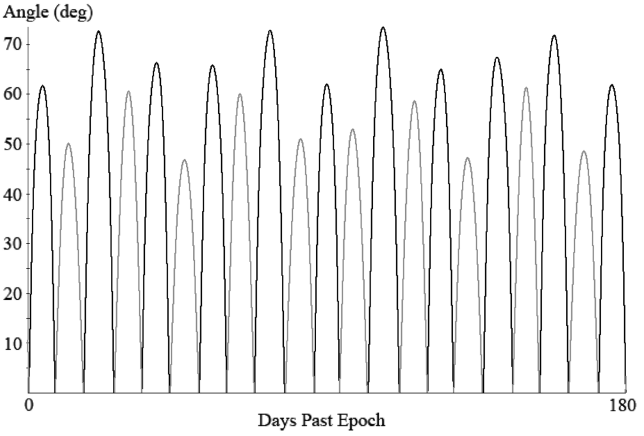

c)

Fig. 13 Sixteen-day L_1 and L_2 vertical orbits: a) two phased spacecraft in orbits from Generator: moon-centered rotating reference frame (top left), x^m-z^m projection (top right), inertial mean J2000 reference frame (center), and z^m displacement from rotating reference frame (bottom); b) STK results: moon-centered rotating frame (top) and moon-centered inertial frame (bottom); and c) elevation of each spacecraft above the horizon as viewed from the Shackleton crater facility vs days past epoch.

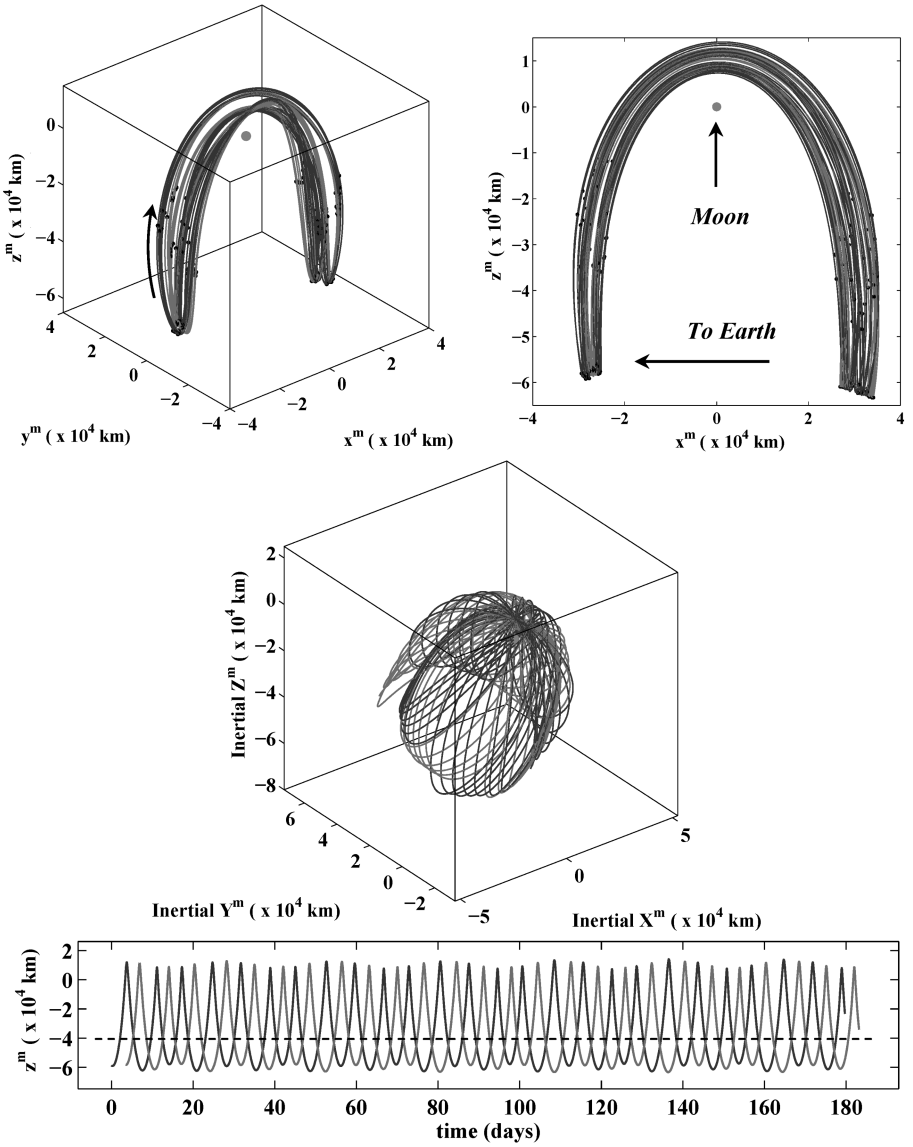

a)

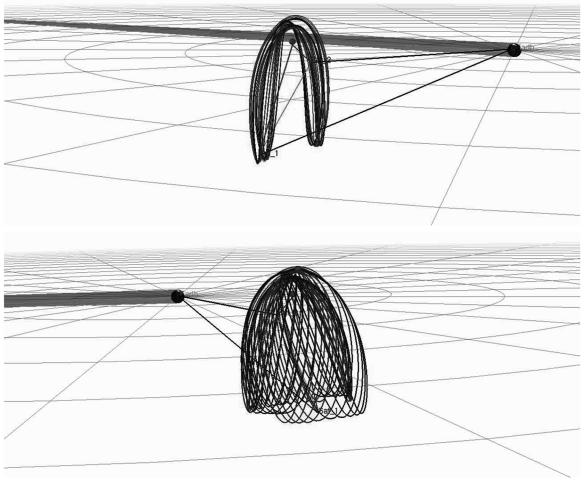

b)

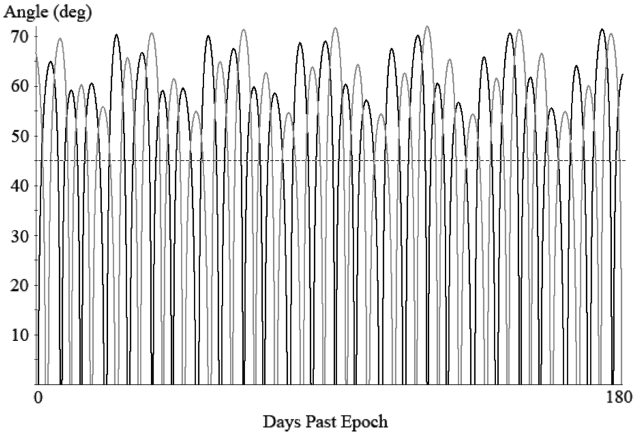

c)

Fig. 14 Fourteen-day L_2 butterfly orbits: a) two phased spacecraft in orbits from Generator: moon-centered rotating reference frame (top left), x^m-z^m projection (top right), inertial mean J2000 reference frame (center), and z^m displacement from rotating reference frame (bottom); b) STK results: moon-centered rotating frame (top) and moon-centered inertial frame (bottom); and c) elevation of each spacecraft above the horizon as viewed from the Shackleton crater facility vs days past epoch.

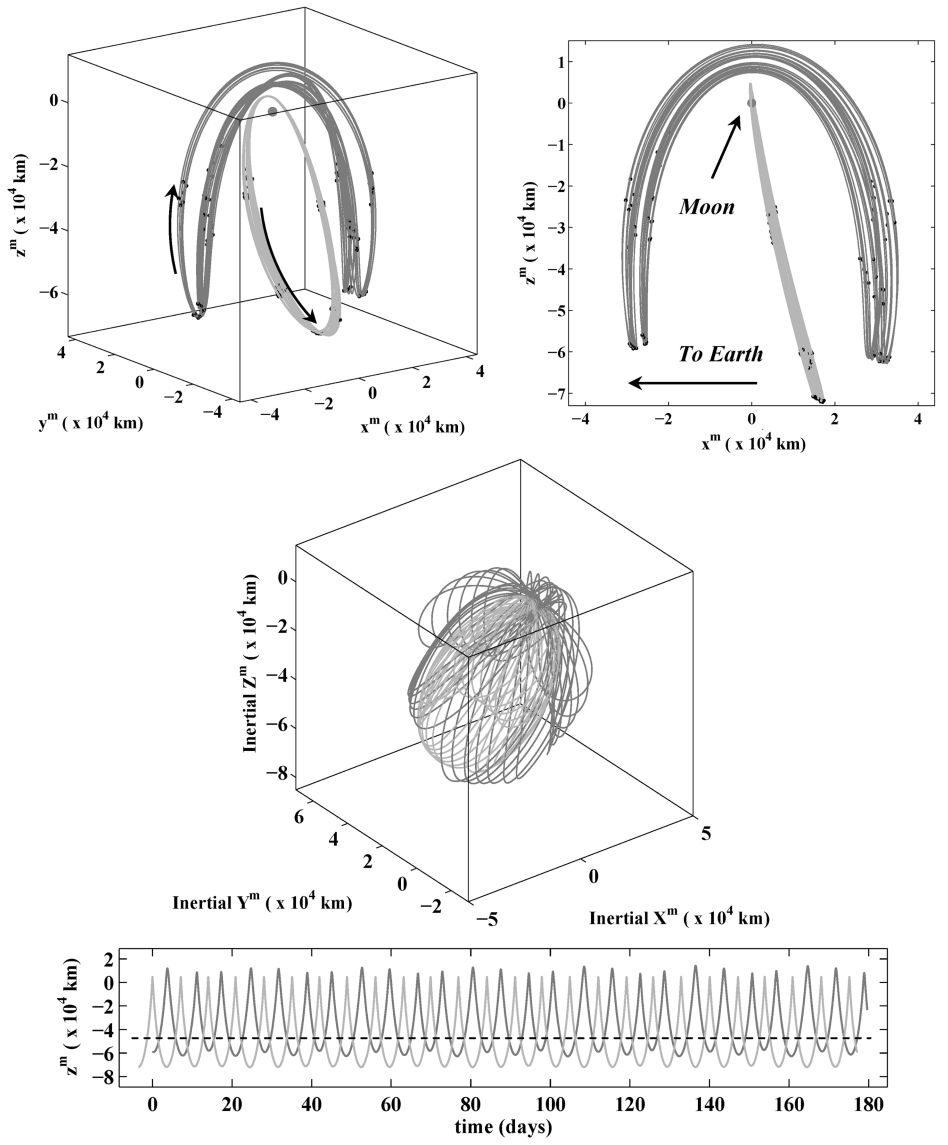

a)

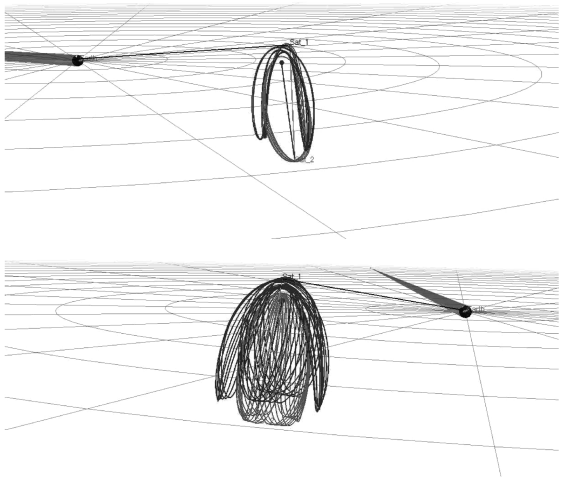

b)

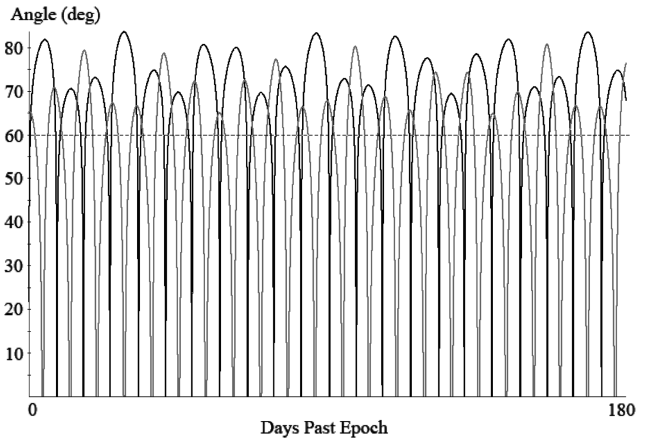

c)

Fig. 15 Seven-day L_2 halo orbit and 14-day L_2 butterfly orbit: a) two phased spacecraft in orbits from Generator: moon-centered rotating reference frame (top left), x^m-z^m projection (top right), inertial mean J2000 reference frame (center), and z^m displacement from rotating reference frame (bottom); b) STK results: moon-centered rotating frame (top) and moon-centered inertial frame (bottom); and c) elevation of each spacecraft above the horizon as viewed from the Shackleton crater facility vs days past epoch.

Table 3 Percent access times for seven-day L_2 halo orbits

Configuration	Facility at Shackleton crater	Earth	Facility at WSTF
Only satellite 1	96.41%	100.00%	47.26%
Only satellite 2	96.37%	100.00%	47.21%
Both satellites	92.78%	100.00%	45.72%
Either satellite	100.00%	100.00%	48.75%

Table 4 Percent access times for eight-day L_1 and L_2 halo orbits

Configuration	Facility at Shackleton crater	Earth	Facility at WSTF
Only L_1 satellite	98.67%	100.00%	46.13%
Only L_2 satellite	93.44%	100.00%	47.43%
Both satellites	92.11%	100.00%	45.46%
Either satellite	100.00%	100.00%	48.10%

Table 5 Percent access times for 16-day L_1 and L_2 vertical orbits

Configuration	Facility at Shackleton crater	Earth	Facility at WSTF
Only L_1 satellite	51.47%	98.27%	49.29%
Only L_2 satellite	47.02%	100.00%	48.04%
Both satellites	0.08%	98.27%	45.19%
Either satellite	98.41%	100.00%	52.14%

Table 6 Percent access times for 14-day L_2 butterfly orbits

Configuration	Facility at Shackleton crater	Earth	Facility at WSTF
Only satellite 1	89.10%	99.45%	46.90%
Only satellite 2	89.15%	99.39%	46.61%
Both satellites	78.25%	98.89%	45.29%
Either satellite	100.00%	100.00%	48.21%

Table 7 Percent access times for seven-day L_2 halo orbit and 14-day L_2 butterfly orbit

Configuration	Facility at Shackleton crater	Earth	Facility at WSTF
Only 14-day satellite	89.22%	99.53%	47.18%
Only seven-day satellite	96.35%	100.00%	46.86%
Both satellites	85.85%	99.53%	45.60%
Either satellite	100.00%	100.00%	48.55%

Finally, Fig. 15 depicts a unique 14-day L_2 butterfly-orbit and seven-day L_2 halo-orbit scenario using two different orbits from two different families. The scenario also exploits a 2:1 ratio between periods. For this specific scenario, the minimum z^m displacement crossover occurs 45,000 km below the fundamental plane (Fig. 15a). Simultaneous coverage occurs for 85.57% of the time between elevations of 0 and 50 deg (see Fig. 15c and Table 7). Furthermore, the spacecraft are in direct line of sight with one another for 99.76% of the simulation time.

C. Station-Keeping Results for Orbits Investigated

Another important factor in determining architectures for lunar south pole coverage is the station-keeping cost associated with each spacecraft. Station-keeping results are obtained in Astrogator Connect using the algorithm represented in Fig. 6. Results for each orbit in Table 1 are specified in Table 8 for one complete year. In general, station-keeping cost increases with stability index. The lowest costs correspond to the seven- and eight-day L_2 near-rectilinear halo orbits, and the highest costs are associated with the 14-day L_1 vertical orbit. Recall that these costs have not been optimized. However, experience suggests that these results are consistent with an impulsive control scheme [20].

V. Conclusions

Orbits from the halo, vertical, and butterfly families in the vicinity of the Earth–moon L_1 and L_2 libration points are selected in the CR3BP for potential lunar south pole coverage options. Orbits with altitudes between 50 and 100,000 km are identified as feasible. Nine different orbits with periods ranging from 7 to 16 days are studied in detail. Two phased spacecraft in a single orbit or in a combination of two different orbits, with periods that are commensurate, ensure adequate coverage of the lunar south pole. The orbit with the desired period is determined in the CR3BP from a corrections process with a periodicity constraint. Multiple revolutions are added and the orbit from the CR3BP is translated to a full-ephemeris model, including solar perturbations, using the Purdue University software Generator. Quasi-periodic orbits from Generator are attainable in STK with only minimal corrections for a complete coverage analysis of the Shackleton crater. Access times with various configurations of Earth-based transmitting sites are also computed. A preliminary station-keeping analysis is available using Astrogator Connect by targeting points along the baseline orbit and perturbing the spacecraft in a direction consistent with the unstable subspace.

Analysis continues to obtain transfers from the Earth to such orbits [32]. In general, the stability index offers information regarding the relative transfer costs of the orbits. In addition, libration-point orbits from other families may also render coverage options for the lunar south pole. The procedure is also easily adaptable for designing feasible architectures for coverage of the north pole. Ultimately, each architecture possesses unique coverage characteristics, station-keeping cost, and transfer cost.

Table 8 Station-keeping results for 1 year (~24 revolutions)

Orbit type	Libration point	Period, days	Stability index	Avg. $3\sigma\|\delta \boldsymbol{V}_i\|$, cm/s	No. of maneuvers	Avg. time between maneuvers, days	Avg. $\|\Delta \boldsymbol{v}_i\|$, m/s	Total $\|\Delta \boldsymbol{v}\|$, m/s
Near-rectilinear halo	L_2	7.0	1.00	2.06	86	4.20	0.057	4.82
Near-rectilinear halo	L_1	8.0	1.25	1.52	55	6.40	0.101	5.54
Near-rectilinear halo	L_2	8.0	1.00	2.18	55	6.40	0.086	4.69
Halo	L_1	12.0	60	3.82	60	6.00	1.106	66.33
Halo	L_2	14.0	115	2.77	156	2.33	0.183	28.47
Vertical	L_1	14.0	690	3.13	68	5.25	2.527	171.82
Butterfly	L_2	14.0	11.3	9.78	78	4.67	0.409	31.86
Vertical	L_1	16.0	370	2.81	91	4.00	0.347	31.55
Vertical	L_2	16.0	515	2.75	60	6.00	1.472	88.32

Acknowledgments

Some portions of this investigation were supported directly by the NASA Academy at NASA Goddard Space Flight Center and at Purdue University. The authors would like to thank Frank Vaughn for the Satellite Tool Kit (STK) model adapted for this study and also Analytical Graphics, Inc., representative Paul Black for his immediate assistance with STK. The majority of this work was completed at the NASA Goddard Space Flight Center in the Flight Dynamics Analysis Branch; contributions were also obtained from studies at Purdue University under contract number NNG05GM76G.

References

[1] Nozette, S., Lichtenberg, C., Spudis, P., Bonner, R., Ort, W., Maleret, E., Robinson, M., and Shoemaker, E., "The Clementine Bistatic Radar Experiment," *Science*, Vol. 274, No. 5292, 1996, pp. 1495–1498. doi:10.1126/science.274.5292.1495

[2] Kozlova, E., "The Presence of Volatiles in the Polar Regions of the Moon," 35th COSPAR Scientific Assembly, Paris, Committee on Space Research Paper COSPAR04-A-04165, 18–25 July 2004.

[3] *The Vision for Space Exploration*, NASA Rept. NP-2004-01-334-HQ, Feb. 2004.

[4] "Space Science Enterprise 2000 Strategic Plan" [online publication], http://spacescience.nasa.gov/admin/pubs/strategy/2000/ [retrieved 11 December 2007].

[5] Szebehely, V., *Theory of Orbits: The Restricted Problem of Three Bodies*, Academic Press, New York, 1967.

[6] Zagouras, C., and Kazantzis, P., "Three-Dimensional Periodic Oscillations Generating from Plane Periodic Ones Around the Collinear Lagrangian Points," *Astrophysics and Space Science*, Vol. 61, No. 2, April 1979, pp. 389–409. doi:10.1007/BF00640540

[7] Breakwell, J., and Brown, J., "The 'Halo' Family of 3-Dimensional Periodic Orbits in the Earth-Moon Restricted 3-Body Problem," *Celestial Mechanics*, Vol. 20, No. 4, 1979, pp. 389–404. doi:10.1007/BF01230405

[8] Robin, I., and Markellos, V., "Numerical Determinations of Three-Dimensional Periodic Orbits Generated from Vertical Self-Resonant Satellite Orbits," *Celestial Mechanics*, Vol. 21, No. 4, May 1980, pp. 395–434. doi:10.1007/BF01231276

[9] Howell, K., and Breakwell, J., "Almost Rectilinear Halo Orbits," *Celestial Mechanics*, Vol. 32, No. 1, January 1984, pp. 29–52. doi:10.1007/BF01358402

[10] Dichmann, D., Doedel, E., and Paffenroth, R., "The Computation of Periodic Solutions of the 3-Body Problem Using the Numerical Continuation Sofware AUTO," *Libration Point Orbits and Applications*, edited by G. Gómez, M. Lo, and J. Masdemont, World Scientific, Hong Kong, 2003.

[11] Farquhar, R., "Lunar Communications with Libration-Point Satellites," *Journal of Spacecraft and Rockets*, Vol. 4, No. 10, 1967, pp. 1383–1384.

[12] Farquhar, R., "The Utilization of Halo Orbits in Advanced Lunar Operations," NASA Goddard Space Flight Center, Rept. TND-365, Greenbelt, MD, 1971.

[13] Grebow, D., "Generating Periodic Orbits in the Circular Restricted Three-Body Problem with Applications to Lunar South Pole Coverage," M.S. Thesis, School of Aeronautics and Astronautics, Purdue Univ., West Lafayette, IN, May 2006.

[14] Moulton, F., *Periodic Orbits*, Carnegie Institution of Washington, Washington, D.C., 1920.

[15] Wilson, R., and Howell, K., "Trajectory Design in the Sun–EARTH-Moon System Using Multiple Lunar Gravity Assists," *Journal of Spacecraft and Rockets*, Vol. 35, No. 2, Mar.–Apr. 1998, pp. 191–198.

[16] Howell, K., and Anderson, J., "Generator User's Guide," Ver. 3.0.2, Purdue Univ., West Lafayette, IN, July 2001.

[17] Ely, T., "Stable Constellations of Frozen Elliptical Inclined Orbits," *Journal of the Astronautical Sciences*, Vol. 53, No. 3, 2005, pp. 301–316.

[18] Ely, T., and Lieb, E., "Constellations of Elliptical Inclined Lunar Orbits Providing Polar and Global Coverage," *Journal of the Astronautical Sciences*, Vol. 54, No. 1, 2006, pp. 53–67.

[19] Simó, C., Gómez, G., Libre, J., and Martínez, R., "Station Keeping of a Quasiperiodic Halo Orbit Using Invariant Manifolds," *Proceedings of the Second International Symposium on Space Flight Dynamics*, SP-255, ESA, Paris, Oct. 1986, pp. 65–70.

[20] Simó, C., Gómez, G., Libre, J., Martínez, R., and Rodríguez, J., "On the Optimal Station Keeping Control of Halo Orbits," *Acta Astronautica*, Vol. 15, Nos. 6–7, 1987, pp. 391–397. doi:10.1016/0094-5765(87)90175-5

[21] Howell, K., and Pernicka, H., "Stationkeeping Method for Libration Point Trajectories," *Journal of Guidance, Control, and Dynamics*, Vol. 16, No. 1, 1993, pp. 151–159.

[22] Howell, K., and Keeter, T., "Station-Keeping Strategies for Libration Point Orbits: Target Point and Floquet Mode Approaches," *Advances in the Astronautical Sciences*, edited by R. Proulx, J. Liu, P. Seidelmann, and S. Alfano, Vol. 89, Plenum Press, New York, 1995, pp. 1377–1396.

[23] Gómez, G., Howell, K., Masdemont, J., and Simó, C., "Station-Keeping Strategies for Translunar Libration Point Orbits," American Astronautical Society Paper 98-168, Feb. 1998.

[24] Scheeres, D., Han, D., and Hou, Y., "The Influence of Unstable Manifolds on Orbit Uncertainty," *Journal of Guidance, Control, and Dynamics*, Vol. 24, No. 3, 2001, pp. 573–585.

[25] Renault, C., and Scheeres, D., "Statistical Analysis of Control Maneuvers in Unstable Orbital Environments," *Journal of Guidance, Control, and Dynamics*, Vol. 26, No. 5, 2003, pp. 758–769.

[26] Folta, D., and Vaughn, F., "A Survey of Earth-Moon Libration Orbits: Station-Keeping Strategies and Intra-Orbit Transfers," AIAA Paper 04-4741, August 2004.

[27] Gómez, G., Libre, J., Martínez, R., and Simó, C., *Dynamics and Mission Design Near Libration Points; Fundamentals: The Case of Collinear Libration Points*, Vol. 1, World Scientific, Singapore, 2001.

[28] Howell, K., and Pernicka, H., "Numerical Determination of Lissajous Trajectories in the Restricted Three-Body Problem," *Celestial Mechanics*, Vol. 41, Nos. 1–4, 1988, pp. 107–124.

[29] Hughes, S., Cooley, D., and Guzmán, J., "A Direct Method for Fuel Optimal Maneuvers of Distributed Spacecraft in Multiple Flight Regimes," American Astronautical Society, Paper 05-158, Jan. 2005.

[30] Marchand, B., Howell, K., and Wilson, R., "An Improved Corrections Process for Constrained Trajectory Design in the *n*-Body Problem," *Journal of Spacecraft and Rockets*, Vol. 44, No. 4, 2007, pp. 884–897.

[31] Marchand, B., and Howell, K., "Aspherical Formations Near the Libration Points in the Sun–Earth/Moon Ephemeris System," American Astronautical Society, Paper 04-157, Feb. 2004.

[32] Ozimek, M., "Low-Thrust Transfer Strategy to Earth-Moon Collinear Libration Point Orbits," M.S. Thesis, School of Aeronautics and Astronautics, Purdue Univ., West Lafayette, IN, Dec. 2006.

C. Kluever
Associate Editor